Competitive Adsorption of Thiolated Polyethylene Glycol and Mercaptopropionic Acid on Gold Nanoparticles Measured by Physical Characterization Methods

ARTICLE *in* LANGMUIR · JUNE 2010

Impact Factor: 4.46 · DOI: 10.1021/la100484a · Source: PubMed

6 AUTHORS, INCLUDING:

Robert I Maccuspie
Natural Immunogenics, Inc.
62 PUBLICATIONS **1,310** CITATIONS
SEE PROFILE

Tae Joon Cho
National Institute of Standards and Technol…
38 PUBLICATIONS **782** CITATIONS
SEE PROFILE

Vincent A. Hackley
National Institute of Standards and Technol…
111 PUBLICATIONS **2,097** CITATIONS
SEE PROFILE

Langmuir
Article
pubs.acs.org/Langmuir

Competitive Adsorption of Thiolated Polyethylene Glycol and Mercaptopropionic Acid on Gold Nanoparticles Measured by Physical Characterization Methods

De-Hao Tsai,[†] Frank W. DelRio,[†] Robert I. MacCuspie,[†] Tae Joon Cho,[†] Michael R. Zachariah,[‡,§] and Vincent A. Hackley*,[†]

[†]*Ceramics Division, and* [‡]*Process Measurements Division, National Institute of Standards and Technology, Gaithersburg, Maryland 20899, and* [§]*University of Maryland, Departments of Mechanical Engineering and Chemistry, College Park, Maryland 20740*

Received February 1, 2010. Revised Manuscript Received April 13, 2010

Competitive adsorption kinetics between thiolated polyethylene glycol (SH-PEG) and mercaptopropionic acid (MPA) on gold nanoparticles (Au-NPs) were studied using a prototype physical characterization approach that combines dynamic light scattering (DLS) and electrospray differential mobility analysis (ES-DMA). The change in hydrodynamic particle size (intensity average) due to the formation of SH-PEG coatings on Au-NPs was measured by DLS in both two-component (Au-NP + MPA or Au-NP + SH-PEG) and three-component (Au-NP +MPA + SH-PEG) systems. ES-DMA was employed to quantify the surface coverage of SH-PEG and establish a correlation between surface coverage and the change in particle size measured by DLS. A change in the equilibrium binding constant for SH-PEG on Au-NPs at various concentrations of SH-PEG and MPA showed that the presence of MPA reduced the binding affinity of SH-PEG to the Au-NP surface. Kinetic studies showed that SH-PEG was desorbed from the Au-NP surface following a second-order desorption model after subsequently introducing MPA. The desorption rate constant of SH-PEG from the Au-NP surface by MPA displacement was strongly affected by the concentration of MPA and the excess SH-PEG in solution.

1. Introduction

Colloidal gold nanoparticles (Au-NPs) are of particular interest in nanomedicine because of many factors, principal among which are their general biocompatibility, ease of surface functionalization (e.g., using thiol chemistry), and tunable surface plasmon resonance (SPR) absorption. These properties are being exploited, for example, in various cancer therapies.[1−12] In addition, Au-NPs can be designed to achieve target-cell-specific uptake for efficient gene therapy via functionalization with small molecular ligands.[1−3,5−8] Among the molecules used for functionalizing Au-NPs, polyethylene glycol (PEG), or more specifically thiolated polyethylene glycol (SH-PEG), is one of the more important and widely used species. For example, PEG-functionalized Au-NPs are presently used for applications such as "immunogold" labeling and as a targeted labeling agent for human carcinoma tissue.[1] The presence of surface-bound SH-PEG has been demonstrated to resist the direct physisorption of proteins onto the surfaces of nanoparticles, thus enhancing particle biocompatibility and the immune response and increasing the residence time in the circulatory system.[1,5−7]

As a result of its widespread use, it is important to know both the adsorbed density and the structural form of SH-PEG on the surfaces of particles because these are indicators of therapeutic performance.[13] Hence, it is necessary to develop methods to characterize both the molecular surface coverage and the subsequent molecular conformation on particles. Moreover, once SH-PEG is present in a multicomponent system (Au-NP + SH-PEG + other molecules present),[1,5−7] the multiple interactions between the particle surface, SH-PEG, and other molecules can evolve and become more complicated. Parameters such as equilibrium binding constants and reaction rate constants (e.g., for adsorption and desorption) are also very important to the design of nanomedicine products. Hence, the development of well-suited quantitative characterization methods to conduct kinetic studies is a necessary step.

Separation-and-analysis methods are commonly used to characterize molecular surface coverage on particles. Briefly, a suspension containing nanoparticles is centrifuged, causing the particle phase to separate from the solution (supernatant). The number of unbound molecules can then be quantified by characterizing the supernatant using one of several analytical techniques

*Corresponding author. E-mail: vince.hackley@nist.gov.

(1) Eck, W.; Craig, G.; Sigdel, A.; Ritter, G.; Old, L. J.; Tang, L.; Brennan, M. F.; Allen, P. J.; Mason, M. D. *ACS Nano* **2008**, *2*, 2263–2272.
(2) Farma, J. M.; Puhlmann, M.; Soriano, P. A.; Cox, D.; Paciotti, G. F.; Tamarkin, L.; Alexander, H. R. *Int. J. Cancer* **2007**, *120*, 2474–2480.
(3) Goel, R.; Swanlund, D.; Coad, J.; Paciotti, G. F.; Bischof, J. C. *Mol. Cancer Ther.* **2007**, *6*, 2039–2047.
(4) Paciotti, G.; Li, Q.; Simpson, B.; Soltesiak, K.; Meyer, L.; Davis, N.; Tamarkin, L. *Eur. Cytokine Network* **1998**, *9*, 536.
(5) Paciotti, G. F.; Myer, L. D.; Kim, T. H.; Wang, S.; Alexander, H. R.; Weinreich, D.; Tamarkin, L. *Clin. Cancer Res.* **2001**, *7*, 3673S–3674S.
(6) Paciotti, G. F.; Myer, L.; Weinreich, D.; Goia, D.; Pavel, N.; McLaughlin, R. E.; Tamarkin, L. *Drug Delivery* **2004**, *11*, 169–183.
(7) Paciotti, G. F.; Kingston, D. G. I.; Tamarkin, L. *Drug Dev. Res.* **2006**, *67*, 47–54.
(8) Park, C.; Youn, H.; Kim, H.; Noh, T.; Kook, Y. H.; Oh, E. T.; Park, H. J.; Kim, C. *J. Mater. Chem.* **2009**, *19*, 2310–2315.
(9) Pissuwan, D.; Valenzuela, S. M.; Miller, C. M.; Killingsworth, M. C.; Cortie, M. B. *Small* **2009**, *5*, 1030–1034.
(10) Visaria, R.; Bischof, J. C.; Loren, M.; Williams, B.; Ebbini, E.; Paciotti, G.; Griffin, R. *Int. J. Hyperthermia* **2007**, *23*, 501–511.
(11) Visaria, R. K.; Griffin, R. J.; Williams, B. W.; Ebbini, E. S.; Paciotti, G. F.; Song, C. W.; Bischof, J. C. *Mol. Cancer Ther.* **2006**, *5*, 1014–1020.
(12) Weinreich, D. M.; Puhlmann, M.; Turner, E. M.; Paciotti, G.; Tamarkin, L.; Myer, L.; Alexander, H. R. *Ann. Surg. Oncol.* **2002**, *9*, S44.
(13) Dobrovolskaia, M. A.; Patri, A. K.; Zheng, J. W.; Clogston, J. D.; Ayub, N.; Aggarwal, P.; Neun, B. W.; Hall, J. B.; Mcneil, S. E. *Nanomed. - Nanotechnol. Biol. Med.* **2009**, *5*, 106–117.

such as ultraviolet−visible light adsorption spectroscopy, chromatography, or fluorimetry.[14−16] By subtracting the number of unbound molecules from the total in solution, the number of adsorbed molecules associated with the particle phase can be quantified. If the total surface area of the nanoparticles is known, then the molecular surface coverage (i.e., the adsorption density) can be obtained. However, the major problem with these separation-and-analysis techniques is accuracy, which can be strongly affected by the excess number of molecules used in the functionalization process (e.g., a 200- to 500-fold molar excess is typically used[17]). Moreover, the sample preparation process is time-consuming and can significantly increase the cycle time of each measurement; this is especially true for particles smaller than about 10 nm that require ultracentrifugation for separating particles from solution.

Ideally, developing direct particle characterization in the context of traditional analytical chemistry methods would be preferred, as is routinely done for small molecules. It has been demonstrated that physical characterization methods can be used for the direct characterization of molecular conjugation.[18−20] The general concept here is to measure the change in the particle's drag force as molecules conjugate onto the surface. The molecular surface coverage may be quantified on the basis of the particle drag and knowledge of the molecular chain length.[18−20]

In the present work, we have employed dynamic light scattering (DLS) in conjunction with electrospray differential mobility analysis (ES-DMA) to characterize the molecular conjugation of Au-NPs. DLS is considered by many to be a standard tool for measuring the average particle size because of its wide availability, simplicity of sample preparation and measurement, relevant size range (from <1 nm to about 2 μm), and in situ measurement capability for fluid-born particles. Another important advantage of using DLS is speed; a single particle size measurement can often be performed in under 2 min, which is beneficial to studying the kinetics of conjugation and the initial stage surface reaction. Even though DLS provides many advantages, the correlation between increased hydrodynamic size measured by DLS and molecular surface coverage is not clearly drawn. To address this limitation, we employ ES-DMA, which offers more straightforward data analysis, as a comparison tool to benchmark the results of DLS and to establish a correlation between surface coverage and the DLS results.

Another objective of this study was to understand the competitive adsorption process between SH-PEG and other potential coligands, such as tumor necrosis factor (TNF), a 17 kDa tumorigenesis-inhibiting protein with a compact structure.[5−7,21−23] For the purpose of examining SH-PEG adsorption/desorption on Au-NPs in the presence of small, compact molecule ligands, mercaptopropionic acid (MPA) was introduced as a proxy to create a three-component system (Au-NP + SH-PEG + MPA). MPA is widely used to bridge proteins and other amine-functionalized molecules onto the surfaces of Au-NPs to form molecular conjugation. In addition, MPA-conjugated Au-NPs have been used as biomarkers of drug-resistant cells.[24] By both DLS and ES-DMA, the equilibrium binding constant of SH-PEG in the presence of MPA was determined. In addition, by introducing MPA into PEG-functionalized Au-NP solutions, the chemical stability of PEG conjugates on the surfaces of Au-NPs was examined and the desorption rate constants were determined.

2. Experimental Section

1. Materials. Commercially available monodisperse citrate-stabilized Au colloids (nominal diameter 30 nm, Ted Pella Inc., Redding, CA) were used without further purification.[25] Thiolated polyethylene glycols (SH-PEG, 1 and 20 kDa, Nanocs, New York, NY; 5 kDa, JenKem Technology USA, Allen, TX) were used in concentrations ranging from 5×10^{-4} to 0.2 mmol/L. Aqueous 3-mercaptopropionic acid (MPA, 99+%, Sigma-Aldrich, St. Louis, MO) was prepared in the concentration range of 0.0287−2.2 mmol/L with filtered deionized water (Aqua Solutions, Jasper, GA). For the sample preparation of conjugated Au-NP, 200 μL of an adsorbate aqueous solution (MPA, SH-PEG, or both) with 5× concentration was first prepared, and then 800 μL of as-received citrate-stabilized Au colloids was added to react with the adsorbates. An aqueous ammonium acetate (99.9%, Sigma-Aldrich, St. Louis, MO) solution was prepared to adjust the ionic strength used in the ES-DMA measurements.

2. Dynamic Light Scattering. DLS measurements were performed using a Zetasizer Nano (Malvern Instruments, Westborough, MA) in backscatter configuration ($\theta = 173°$) at a laser wavelength of $\lambda_0 = 633$ nm. Measurement protocols used in this study are described elsewhere,[26] and measurements were made over ~2 min by collecting no less than 12 runs of submeasurements at a constant temperature of 21.0 °C ± 0.1 °C. No additional purification step was used following the conjugation of Au-NPs prior to DLS measurements (i.e., no further removal of the unbound molecules).

In principle, DLS characterizes the Brownian motion of particles in solution and correlates this motion to particle size. Particle motion results in fluctuations in the scattered light when a small scattering volume is imaged. These fluctuations can be autocorrelated over a very short time interval from which the particle diffusion coefficient, D (and subsequently the hydrodynamic particle size, $d_{p,h}$), is extracted. All size information for the ensemble of particles is contained within a single correlation curve.[27,28] The Stokes−Einstein relationship (eq 1) is the basis for extracting size from the DLS-measured diffusion coefficient.

$$d_{p,h} = \frac{kT}{3\pi\eta D} \tag{1}$$

where η is the viscosity of the solution, k is Boltzmann's constant, and T is the temperature of the measurement. In the Rayleigh limit, the intensity of light scattered by a single particle is

(14) Kandori, K.; Mizumoto, S.; Toshima, S.; Fukusumi, M.; Morisada, Y. *J. Phys. Chem. B* **2009**, *113*, 11016–11022.
(15) Demers, L. M.; Mirkin, C. A.; Mucic, R. C.; Reynolds, R. A.; Letsinger, R. L.; Elghanian, R.; Viswanadham, G. *Anal. Chem.* **2000**, *72*, 5535–5541.
(16) Kandori, K.; Fudo, A.; Ishikawa, T. *Phys. Chem. Chem. Phys.* **2000**, *2*, 2015–2020.
(17) Woehrle, G. H.; Brown, L. O.; Hutchison, J. E. *J. Am. Chem. Soc.* **2005**, *127*, 2172–2183.
(18) Pease, L. F.; Tsai, D. H.; Zangmeister, R. A.; Zachariah, M. R.; Tarlov, M. J. *J. Phys. Chem. C* **2007**, *111*, 17155–17157.
(19) Pease, L. F.; Lipin, D. I.; Tsai, D. H.; Zachariah, M. R.; Lua, L. H. L.; Tarlov, M. J.; Middelberg, A. P. J. *Biotechnol. Bioeng.* **2009**, *102*, 845–855.
(20) Tsai, D. H.; Zangmeister, R. A.; Pease, L. F.; Tarlov, M. J.; Zachariah, M. R. *Langmuir* **2008**, *24*, 8483–8490.
(21) Smith, R. A.; Baglioni, C. *J. Biol. Chem.* **1989**, *264*, 14646–14652.
(22) Smith, R. A.; Baglioni, C. *J. Biol. Chem.* **1987**, *262*, 6951–6954.
(23) Smith, R. A.; Kirstein, M.; Fiers, W.; Baglioni, C. *J. Biol. Chem.* **1986**, *261*, 4871–4874.
(24) Hu, F. Q.; Ran, Y. L.; Zhou, Z. A.; Gao, M. Y. *Nanotechnology* **2006**, *17*, 2972–2977.
(25) Certain commercial equipment, instruments, or materials are identified in this report to specify the experimental procedure adequately. Such identification is not intended to imply a recommendation or endorsement by the National Institute of Standards and Technology nor is it intended to imply that the materials or equipment identified are necessarily the best available for the purpose.
(26) Hackley, V. A.; Clogston, J. D. NIST-NCL Joint Assay Protocol PCC-1, Nanotechnology Characterization Laboratory (ncl.cancer.gov); **2007**.
(27) ISO 22412:2008E. Particle size analysis - dynamic light scattering (DLS); **2008**.
(28) Pusey, P. N.; Koppel, D. E.; Schaefer, D. W.; Camerini, R. D.; Koenig, S. H. *Biochemistry* **1974**, *13*, 952–960.

proportional to its volume squared. This means that the average size of a mixture of differently sized particles determined by light scattering will also be weighted by the volume squared and is called the *z*-average particle size, $d_{p,hz}$, given by[29]

$$d_{p,hz} = \frac{kT}{3\pi\eta\bar{D}} = \frac{\sum N_i d_{p,h,i}^{7}}{\sum N_i d_{p,h,i}^{6}} \quad (2)$$

where N_i is the number of particles of type i having hydrodynamic diameter $d_{p,h,i}$. $\bar{D}$ is the *z*-average particle diffusion coefficient.

To obtain $\bar{D}$ and $d_{p,hz}$ from the correlation data measured by DLS, the most reliable and widely used algorithm is based on the cumulant analysis method,[26−28,30] which involves a second-order polynomial expansion of the correlation function,

$$\ln[G(\tau) - 1] = \ln[\beta|g(\tau)|^2] = \ln\beta - 2\bar{\Gamma}\tau + \mu_2\tau^2 \quad (3)$$

where $G(\tau)$ is the normalized intensity autocorrelation function measured in DLS, τ is the delay time, $g(\tau)$ is the electric field autocorrelation function, and β is an instrument-related constant with a value close to unity . The parameter $\bar{\Gamma}$ is the mean decay rate, which is equal to $\bar{D}q^2$, where q is the modulus of the scattering vector

$$q = \frac{4\pi n}{\lambda_0}\sin(\theta/2) \quad (4)$$

where n is the refractive index of the solution and θ is the scattering angle. In the present system, $q = 2.64 \times 10^7\ m^{-1}$. The moment term μ_2 is equivalent to the variance associated with $\bar{\Gamma}$, where $\mu_2/\bar{\Gamma}^2$ is referred to as the polydispersity index. On the basis of DLS correlation data, a non-negative least-squares (NNLS) regularization algorithm provided by the instrument manufacturer can be used to calculate a size distribution. However, the resolution by NNLS is user-adjustable and inherently limited, especially when the particle size distribution is broad or multimodal.

3. Electrospray Differential Mobility Analysis. In many ways analogous to mass spectrometry, ES-DMA separates aerosol particles on the basis of their surface-to-charge ratio. Details of the ES-DMA experimental setup have been described in previous publications.[20,31,32] Briefly, operating with an applied voltage of 2 kV to 3 kV, a particle suspension (Au colloids in the present case) is sprayed in cone-jet mode and then the aerosol stream is passed through a housing containing a radioactive Po-210 source that reduces the highly charged droplets to droplets that are primarily either neutral, have a single negative charge, or have a single positive charge.[31] After solvent evaporation, the dried, positively charged particles are then separated within the differential mobility analyzer (DMA) on the basis of their electrical mobility, Z_e, which is inversely proportional to the projected area of the particles.

$$Z_e = \frac{n_e e C_c}{3\pi\eta_g d_{p,m}} \approx \frac{n_e e}{d_{p,m}^{2}} \quad (5)$$

where $d_{p,m}$ is the mobility diameter of a particle, η_g is the viscosity of the carrier gas, and C_c is the slip correction factor of a particle in a carrier gas.[33] For a particle size of less than about 100 nm, $C_c \approx d_{p,m}^{-1}$. n_e is the number of unit charges, and e is the elemental charge (1.6×10^{-19} C).

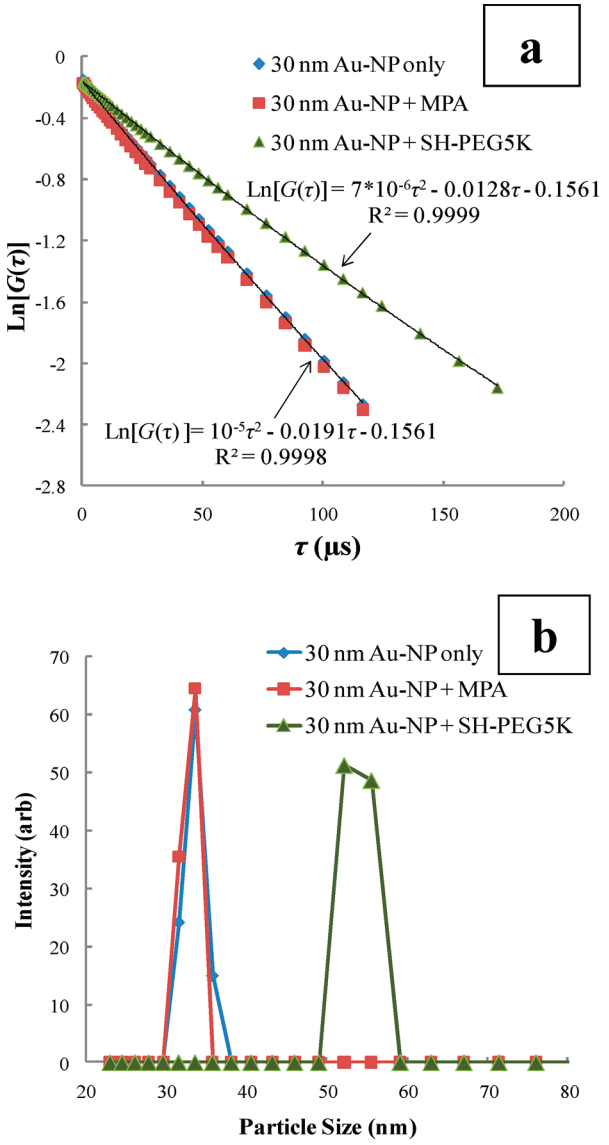

Figure 1. Characterization of the two-component system by DLS. Au-NPs (30 nm) conjugated with SH-PEG5K or MPA. (a) Cumulant analysis. (b) NNLS analysis. The concentration of SH-PEG5K is 0.20 mmol/L, and the concentration of MPA is 0.287 mmol/L.

The differential mobility analyzer acts as a narrow band-pass filter, transmitting aerosolized colloids of a specific size to a condensation particle counter, and the number of particles passing the detector is recorded. The electrical mobility of particles exiting DMA, $Z_{e,out}$, can be calculated from the particle's trajectory in the DMA. In general,

$$Z_{e,out} \approx \frac{Q_{sh}}{V_e} \quad (6)$$

where V_e is the voltage applied in the axial direction of the DMA, determining the particle's axial velocity. Q_{sh} is the sheath flow rate in the DMA used to determine the particle's lateral velocity. Under a constant Q_{sh}, increasing V_e results in decreasing $Z_{e,out}$ (or increasing $d_{p,m}$) delivered to the condensation particle counter. By combining eqs 5 and 6, the correlation of the mobility diameter measured by ES-DMA becomes $d_{p,m} \approx (V_e/Q_{sh})^{0.5}$.

To achieve sufficient resolution and stability from the DMA, the ratio of sheath-to-aerosol flow rates was fixed at a value of 30. On the basis of the operating conditions of the DMA, the

(29) Min, G. K.; Bevan, M. A.; Prieve, D. C.; Patterson, G. D. *Colloids Surf., A* **2002**, *202*, 9–21.
(30) ISO 13321:1996(E). Particle size analysis - photon correlation spectroscopy; **1996**.
(31) Kim, S. H.; Woo, K. S.; Liu, B. Y. H.; Zachariah, M. R. *J. Colloid Interface Sci.* **2005**, *282*, 46–57.
(32) Tsai, D. H.; Pease, L. F.; Zangmeister, R. A.; Tarlov, M. J.; Zachariah, M. R. *Langmuir* **2009**, *25*, 140–146.
(33) Hinds, W. C. *Aerosol Technology*, 2nd ed.; Wiley: New York, 1999.

theoretical fwhm in the size distribution yields 30 ± 0.5 nm for 30 nm particles. Under these conditions, data were collected with a scanning step size of 0.2 nm for 20 s, where the uncertainty contributed by the DMA is less than 0.3 nm. Thus, the width of the peaks in the resulting mobility spectra results primarily from the real distribution in particle size. The mobility diameter distribution of the Au-NPs was obtained from the ion-mobility spectrum for positively charged particles by correcting each data point for the charging efficiency. To avoid unwanted salts and unbound SH-PEG precipitating onto the Au-NP surface, more than 99.95% of the supernatant containing excess SH-PEG was removed by centrifugation and replaced with a 2 mmol/L ammonium acetate aqueous solution.

3. Results and Discussion

1. Two-Component System. We begin by examining the application of DLS to study the interaction between a single molecule (SH-PEG or MPA) and Au-NPs (two-component system). Figure 1a compares the measured autocorrelation functions (in semilogarithmic form) for Au-NPs, Au-NPs with SH-PEG, and Au-NPs with MPA, all fitted by a second-order polynomial. After reacting with 0.20 mmol/L of 5 kDa SH-PEG (defined as SH-PEG5K), the τ range necessary to observe the decay of $G(\tau)$ has significantly increased compared to the decay before SH-PEG5K conjugation, indicating a measurable decrease in the mean diffusion coefficient of the particles. Using the first-order polynomial coefficient ($2\bar{\Gamma}$), we calculated the mean diffusion coefficient, $\bar{D}$, and z-average particle size, $d_{p,hz}$. After conjugating with SH-PEG5K, the increase in $d_{p,hz}$, or $\Delta d_{p,hz}$, was observed to be 20 nm ± 0.4 nm on the basis of at least three replicate measurements. At the same time, the polydispersity index derived from the second-order coefficient of the cumulants analysis did not increase following conjugation (i.e., the variance of the distribution is unchanged). This suggests that the observed $\Delta d_{p,hz}$ was caused by a homogeneous change in particle size resulting from ligand adsorption and was not a result of particle agglomeration. In contrast, there was no significant change in the autocorrelation function after conjugating with MPA; (i.e., any increase in the physical size of the particles accompanying conjugation with MPA was not measurable within the resolution limit of DLS).

In addition to applying the cumulants analysis, a non-negative least-squares (NNLS) regularization algorithm was used to calculate a size distribution from the DLS correlation data. Because the Au-NPs were monomodal with a relatively narrow size variance without the presence of aggregates, the regularization parameter in the NNLS algorithm was set at a value appropriate for high-resolution analysis (i.e., minimal smoothing). Just as with the cumulant results, NNLS size distributions (Figure 1b) were almost identical for MPA-conjugated and unconjugated Au-NPs, with a significant increase in the central tendency of the distribution after conjugation with SH-PEG5K.

2. Three-Component System. Next, the three-component system was studied to determine the competitive adsorption effects between SH-PEG5K and MPA on Au-NPs. Because MPA and SH-PEG5K have shown very different responses of $\Delta d_{p,hz}$ after conjugation (Figure 1), DLS should be able to characterize the relative amounts of MPA and SH-PEG5K when both are adsorbed on a Au-NP simultaneously. As discussed with respect to Figure 1, conjugation with MPA did not increase the measured hydrodynamic size of Au-NPs, indicating that in the three-component system $\Delta d_{p,hz}$ should increase only through the adsorption of SH-PEG5K to the Au-NP surface. In other words, if $\Delta d_{p,hz}$ particles decreased relative to fully conjugated SH-PEG-AuNPs, then this must be the result of MPA molecules inhibiting

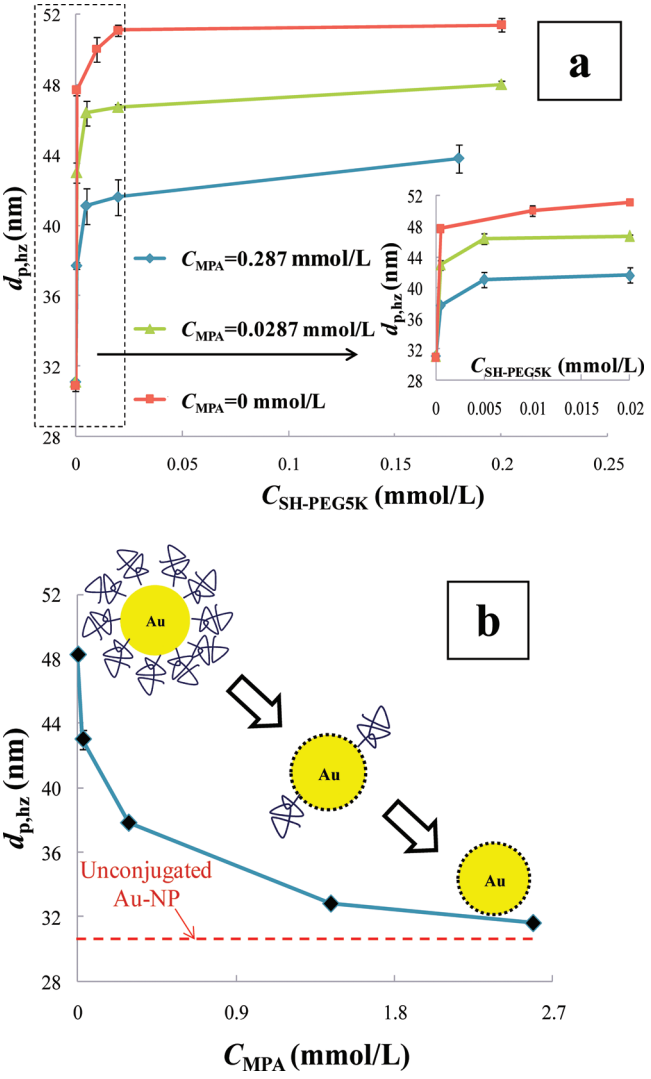

Figure 2. Characterization of the z-average size in a three-component (SH-PEG5K, MPA, Au-NP) system by DLS. (a) Particle size vs concentration of SH-PEG5K, $C_{SH-PEG5K}$, as a function of MPA concentration, C_{MPA}: 0, 0.0287, and 0.287 mmol/L. (b) Effect of MPA concentration on the particle size of SH-PEG5K-conjugated Au-NPs. $C_{SH-PEG5K} = 5 \times 10^{-4}$ mmol/L. Error bars represent one standard deviation of triplicate measurements. Lines are present to guide the eyes.

the adsorption of SH-PEG5K on the Au-NPs through direct solution-phase interactions or by occupying some of the available sites on the particle surface.

Figure 2a shows the particle size measured by DLS under various concentrations of SH-PEG5K and MPA. Here SH-PEG5K and MPA were first mixed, and then the Au-NPs were subsequently added to the solution containing the adsorbates. Without MPA, $d_{p,hz}$ of Au-NPs was increased to about 48.5 nm even at very low SH-PEG5K concentration (5×10^{-4} mmol/L). As the concentration of SH-PEG5K increased from 5×10^{-4} to 0.2 mmol/L, $d_{p,hz}$ approached a plateau value of ~50 nm. In contrast, as the MPA concentration increased from 0 to 0.328 mmol/L, the $d_{p,hz}$ versus SH-PEG5K concentration curve shifted markedly toward smaller particle sizes, suggesting that MPA was occupying surface sites otherwise available for SH-PEG5K adsorption. Indeed, as shown in Figure 2b, $\Delta d_{p,hz}$ was inversely proportional to the concentration of MPA, showing clearly that the SH-PEG5K conjugation was strongly inhibited in the presence of MPA.

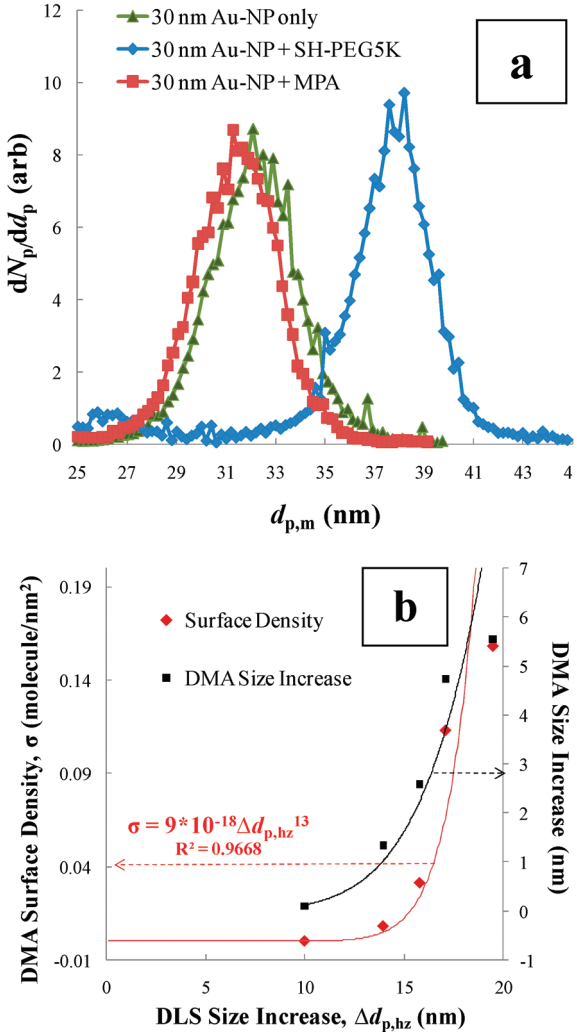

Figure 3. Characterization of particle size distribution and molecular surface coverage by ES-DMA. (a) Particle size distribution under three different experimental conditions. For comparison, $d_{p,hz}$ measured by DLS for Au-NP only and Au-NP + MPA was 31 nm and that for Au-NP + SH-PEG5K was 50 nm. The concentration of MPA was 0.287 mmol/L, and the concentration of SH-PEG5K was 0.20 mmol/L. (b) Summary of DLS vs ES-DMA. The black curve represents the correlation of increased particle size measured by ES-DMA vs that measured by DLS. The red curve represents the surface density of SH-PEG5K vs the increased size measured by DLS. To extrapolate σ as the value close to zero, both correlation curves were obtained by power-series curve fitting.

To understand the competitive adsorption between SH-PEG and MPA better, we quantified the SH-PEG surface coverage, σ, over various concentrations of SH-PEG5K and MPA. ES-DMA was used to quantify the surface coverage of SH-PEG5K and to find a correlation between σ and $\Delta d_{p,hz}$. Figure 3a presents the typical particle size distributions measured by ES-DMA over various experimental conditions. Similar to the results from DLS measurements, we also observed a significant increase in particle mobility size, $\Delta d_{p,m}$, after conjugation with SH-PEG5K, but the apparent particle size decreased 0.5 nm after conjugation with MPA. One possible explanation for a small, negative $\Delta d_{p,m}$ could arise from the variation of the instrument reproducibility itself (±0.3 nm). Another possible explanation might involve a conformational difference between MPA and citrate ions in the dried (aerosol) state. Nevertheless, the increase in particle size measured by ES-DMA can be unequivocally attributed to SH-PEG5K conjugation, and aggregation can be ruled out.

From the mobility particle size distribution we calculated the number-average $d_{p,m}$ of these functionalized Au-NPs according to

$$d_{p,m} = \frac{\sum N_{m,i} d_{p,m,i}}{\sum N_{m,i}} \quad (7)$$

where $N_{m,i}$ is the number of particles of type i having mobility diameter $d_{p,m,i}$. Subsequently, the surface coverage of SH-PEG5K on Au-NPs can be calculated from the increase in the cross-sectional area of particles by SH-PEG5K conjugation. If the molecular surface density of SH-PEG5K allows for sufficient space between SH-PEG5K, the bases of SH-PEG5K will adopt a random coil configuration to maximize entropy and the coating thickness should be proportional to the linear end-to-end distance, $\langle x^2\rangle^{0.5}$, of SH-PEG5K (random-walk radius). We employ a previously developed analytical model,[18]

$$\sigma = \frac{[(d_{p,m}+\Delta d_{p,m})^2 - d_{p,m}{}^2]^2}{[2d_{p,m}\langle x^2\rangle]^2} \quad (8)$$

For freely jointed Gaussian chains, the random-walk radius of SH-PEG, $\langle x^2\rangle^{0.5}$, is given by[18]

$$\langle x^2\rangle^{0.5} = cN_b{}^a N_k{}^a l_b \quad (9)$$

where c is the interaction constant between the polymer and the particle surface (normally $c = 0.62$ for end-anchored polymers), l_b is the length of the monomer segment (0.44 nm), N_k is the number of statistical bases per segment, N_b is the number of segments per polymer, and a is adjusted by the interaction with the solvent. Typically $a = 0.5$ for a normal solvent or under dry conditions[18] and can be as high as 0.6 if a higher affinity exists for the solvent.[34] PEG is a hydrophilic polymer, and in an aqueous solution, it will have a larger random-walk radius than in the dried state.[34] For SH-PEG5K, the calculated random-walk radius is 3.7 nm under dry conditions and 6.2 nm in water.

For an MPA concentration of 0.287 mmol/L, we observed a significant increase in $d_{p,hz}$ (≈10 nm) based on DLS in the presence of 5×10^{-4} mmol/L SH-PEG5K but almost no increase in $d_{p,m}$ derived from ES-DMA. In comparing $\Delta d_{p,hz}$ and $\Delta d_{p,m}$ as shown in Figure 3b, when $\Delta d_{p,hz} \leq 10$ nm, we did not observe any significant change in particle size measured by ES-DMA ($\Delta d_{p,m} \approx 0$). The principal reason for the difference between DLS and ES-DMA is the measurement condition. Because DLS measures the hydrodynamic size in a fluid environment, it is expected to measure a significantly larger increase in particle size because of the larger random-walk radius of PEG accompanied by the solvation of the polymer chain. In contrast, ES-DMA measures the particle size in a dried (aerosol) form in which the adsorbed PEG molecules will be collapsed, resulting in a smaller random-walk radius than in solution.

To understand further the effect of the environment on the molecular conformation, we compared the surface density of SH-PEG5K calculated from $\Delta d_{p,m}$ to the change in particle size measured by DLS. An empirical correlation of σ versus $\Delta d_{p,hz}$ was

(34) Hill, R. J. *Phys. Rev. E* **2004**, *70*, 051406.

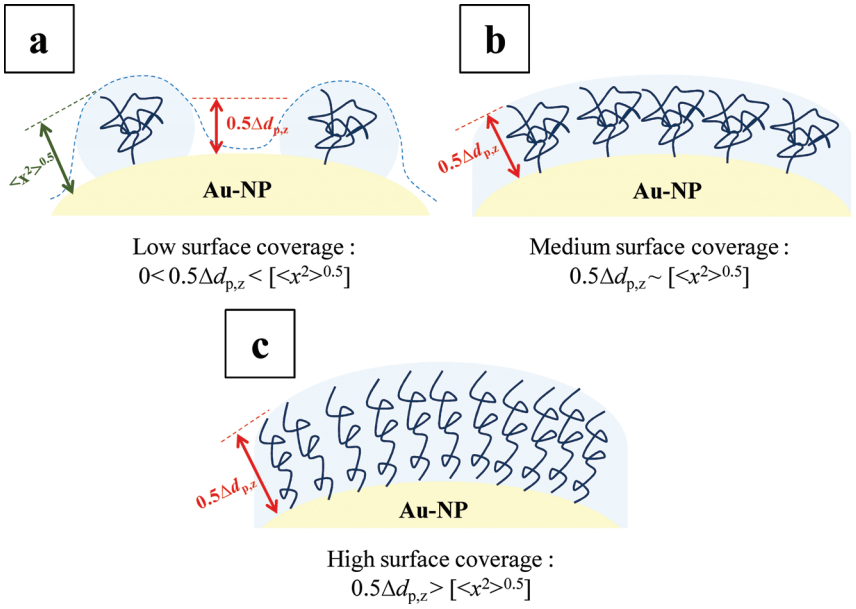

Figure 4. Conceptual diagram of a PEG-functionalized Au-NP measured in the fluid. (a) Low-surface-coverage regime, $\sigma < 1/\langle x^2 \rangle$. (b) Medium-surface-coverage regime, $\sigma \approx 1/\langle x^2 \rangle$. (c) High-surface -coverage regime, $\sigma > 1/\langle x^2 \rangle$.

obtained from Figure 3b, with $\sigma = 9 \times 10^{-18} (\Delta d_{p,hz})^{+13}$. Even at very low surface coverage ($\sigma < 0.01$ nm^{-2}), we still observed a significant change in $d_{p,hz}$, illustrating that DLS is very sensitive to the presence of SH-PEG5K in the low-surface-coverage regime where the hydrodynamic radius is a strong function of surface coverage. Figure 4 displays a conceptual model of PEG-conjugated Au-NPs under the fluid condition. SH-PEG will preferably bind to the particle surface via a reactive thiol−Au bond. After adsorbing to the Au-NPs, individual hydrophilic SH-PEG chains will extend into the adjacent solution and therefore will provide no significant driving force for multilayer formation via hydrophobic or electrostatic attraction.[34,35] Even when the surface coverage of SH-PEG is relatively low ($\sigma \ll 1/\langle x^2 \rangle$), the increase in size can still be significant (Figure 4a). When the surface coverage is increased to $1/\langle x^2 \rangle$ (i.e., 0.03 nm^{-2}), the increased particle size should be about twice the random-walk radius (Figure 4b). When the separation distance between neighboring adsorbed PEG molecules is less than the random-walk radius of the PEG, the SH-PEG chain must expand out from the Au-NP surface because the lateral separation distance between the individual SH-PEG chains is fixed.[35] As the surface coverage continues to increase, SH-PEG at the surface of the Au-NPs assumes a more vertically aligned conformation (Figure 4c); as a result, the increase in particle size can be greater than $2\langle x^2 \rangle^{0.5}$.

In contrast, ES-DMA measures the particle size in the dried state. Hence, the differences were due to not only a smaller random-walk radius but also to the fact that there is no bound water along the SH-PEG chain. At low molecular surface coverage, the increase in particle size due to the conjugate was not significant compared to the overall aerodynamic drag from the particle itself.

To confirm the conceptual model described in Figure 4, SH-PEGs with a relative molecular mass[36] (M_r) of 1 kDa (SH-PEG1K), 5 kDa (SH-PEG5K), and 20 kDa (SH-PEG20K) were studied. In a fluid, the random-walk radii for SH-PEG1K and SH-PEG20K were 2.3 and 14.2 nm, respectively, whereas in the dried state, the random-walk radii were 1.6 nm and 7.3 nm, respectively. Figure 5 compares the increases in particle size measured by both DLS and ES-DMA. In the DLS measurements, increasing M_r increased the particle size significantly and was proportional to the trend of the random-walk radius. However, the trend measured by ES-DMA differed from that measured by DLS; $\Delta d_{p,m}$ increased as M_r increased from 1 kDa to 5 kDa but decreased as M_r increased from 5 kDa to 20 kDa. By converting $\Delta d_{p,m}$ to σ using $\sigma = 9 \times 10^{-18} (\Delta d_{p,hz})^{+13}$, σ was calculated to be 1.3 nm^{-2} for $M_r = 1$ kDa, 0.2 nm^{-2} for $M_r = 5$ kDa, and 4.6×10^{-3} nm^{-2} for $M_r = 20$ kDa. Thus, as M_r increased, σ decreased, suggesting that steric repulsion retards the surface reaction. For SH-PEG with a higher M_r, because of steric hindrance between polymer chains it is more difficult to reach the bare surface of the Au-NPs in the presence of conjugated SH-PEG. In DLS measurements, the measured particle size is defined by an envelope encompassing the core Au-NP, the adsorbed SH-PEG, and entrained solvent. Hence, the impact of molecular surface coverage (i.e., adsorption density) on the increase in particle size may

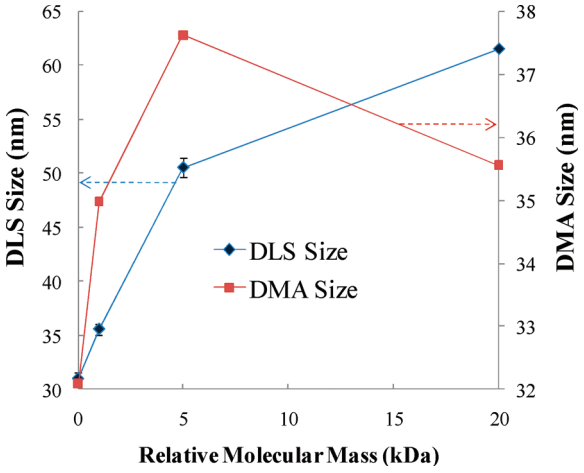

Figure 5. Particle size measurement using SH-PEG as a function of the relative molecular mass. Measurements were carried out by both DLS and ES-DMA. Lines are present to aid viewing.

(35) Netz, R. R.; Andelman, D. *Phys. Rep.* **2003**, *380*, 1–95.
(36) http://goldbook.iupac.org/R05271.html .

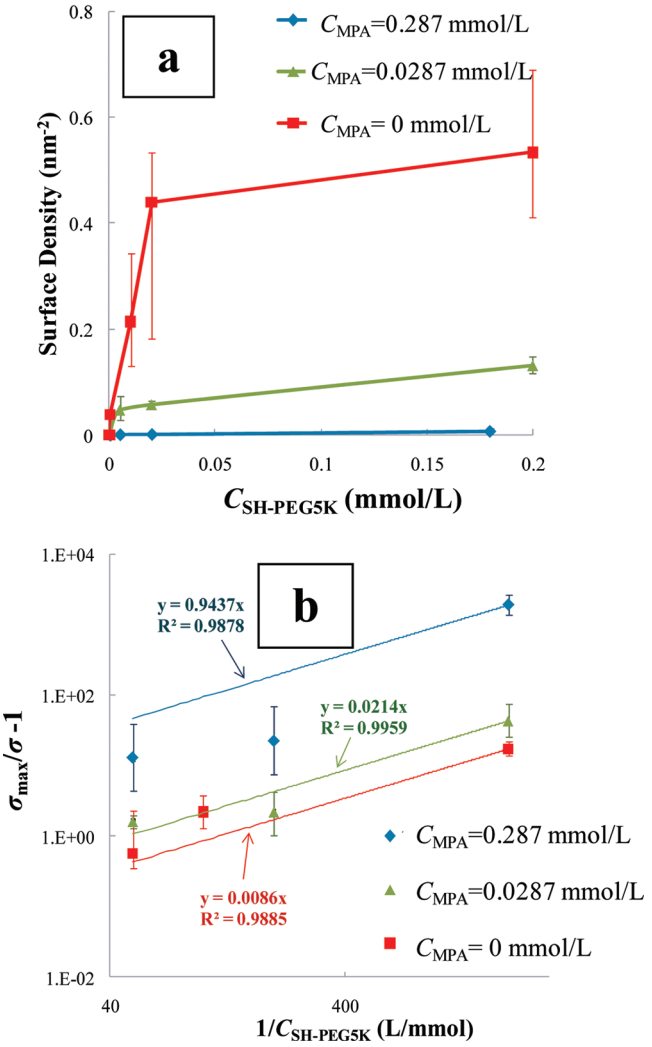

Figure 6. Adsorption of SH-PEG5K in the three-component system. (a) Adsorption isotherms for SH-PEG5K under three different concentrations of MPA: 0, 0.0287, and 0.287 mmol/L. Lines are present to guide the eyes. (b) Langmuir fit to the data of Figure 6a. The slope is $1/K$, where K is the equilibrium binding constant of SH-PEG5K on Au-NPs.

not be as significant compared with the length of the molecule used for conjugation (or the random-walk radius). This result confirms the conceptual model that the random-walk radius is the dominant factor contributing to $\Delta d_{p,hz}$.

By using the correlation between $\Delta d_{p,hz}$ and σ, we can convert the curves of $d_{p,hz}$ versus $C_{SH-PEG5K}$ shown in Figure 2b to adsorption isotherms, assuming that the equilibrium concentration of SH-PEG5K in solution (unbound) is close to the initial concentration in solution ($C_{SH-PEG5K}$). Because of the strong S−Au binding energy (>100 kJ/mol) between adsorbed SH-PEG5K and Au-NP, the mechanism of adsorption for SH-PEG5K to Au-NPs can be classified as chemisorption.[20] As shown in Figure 6a, the adsorption curves do follow a Langmuir-like isotherm (i.e., chemisorbed monolayer). At higher $C_{SH-PEG5K}$, the surface density of SH-PEG5K continued to increase, but with a smaller slope. This result suggests that steric interactions may affect the adsorption density or possibly that physisorption is involved when surface coverage approaches a maximum; however, the Langmuir model assumes surface monolayer coverage but excludes interactions between adjacent adsorbate molecules and thus may not be the optimum model for this system. With this potential limitation in mind, the Langmuir correlation[37] was nevertheless used to obtain the equilibrium binding constant, K.

$$\frac{\sigma_{max}}{\sigma} - 1 = \frac{1}{K^{*}C_{SH-PEG5K}} \qquad (10)$$

where σ_{max} is the maximum surface density of SH-PEG5K. Figure 6b displays the Langmuir fits for three different MPA concentrations (C_{MPA}). From the slope, K was found to be 1.16×10^5 L/mol for C_{MPA} = 0 mmol/L, 4.67×10^4 L/mol for C_{MPA} = 0.0287 mmol/L, and 1.06×10^3 L/mol for C_{MPA} = 0.287 mmol/L. The surface binding constants for SH-PEG5K decreased as C_{MPA} increased, quantitatively expressing the inhibited adsorption of SH-PEG5K to Au-NPs in the presence of MPA.

3. Kinetic Study of SH-PEG5K Desorption from Au-NPs by MPA. We now turn our attention to the chemical stability of SH-PEG5K binding on Au-NPs. Au-NP suspensions were prepared at three different initial values of $C_{SH-PEG5K}$. Following conjugation by SH-PEG5K, MPA was subsequently introduced into the PEG-functionalized Au-NP suspension. As shown in Figure 7a, $d_{p,hz}$ decreased significantly upon addition of MPA, especially during the first 60 min, which indicates that SH-PEG5K was displaced from the surface of Au-NPs. After 60 min, $d_{p,hz}$ was relatively constant, indicating that the displacement reaction slowed because of an increase in unbound SH-PEG5K, driving the reaction more toward the direction of SH-PEG5K adsorption.

After converting $\Delta d_{p,hz}$ to σ, the desorption rate of SH-PEG5K by MPA-induced displacement can be expressed in terms of the change in the surface density,

$$\frac{d\sigma}{dt} = -k_d\sigma^y \qquad (11)$$

where k_d is the rate constant of SH-PEG5K desorption, t is the reaction time, and y is the order of the reaction. For a large initial surface coverage, σ_0, of SH-PEG5K ($\sigma_0 = 0.1-1$ nm^{-2}, as shown in Figure 4c), the neighboring SH-PEG5K molecules may interact with each other during desorption. Hence, it is reasonable to assume that the desorption of SH-PEG5K from Au-NPs is a second-order reaction. By integrating eq 11 with $y = 2$ to express the second-order kinetics, we obtain

$$\frac{1}{\sigma} - \frac{1}{\sigma_0} = k_d t \qquad (12)$$

As shown in Figure 7b, the model is in good agreement with the data for $y = 2$. We obtain $k_d = 1.61$ nm^2/min when $C_{SH-PEG5K} = 5 \times 10^{-4}$ mmol/L, k_d = 0.70 nm^2/min when $C_{SH-PEG5K} = 1 \times 10^{-2}$ mmol/L, and k_d = 0.33 nm^2/min when $C_{SH-PEG5K}$ = 0.20 mmol/L. Increasing $C_{SH-PEG5K}$ results in lower k_d values ($k_d \approx C_{SH-PEG5K}{}^{-0.27}$).

In contrast, increasing C_{MPA} increased the desorption rate of SH-PEG5K. As shown in Figure 7c, for $C_{SH-PEG5K} = 1 \times 10^{-2}$ mmol/L, $\Delta d_{p,hz}$ decreased significantly in the first 10 min for $C_{MPA} \geq 0.287$ mmol/L but remained relatively constant for C_{MPA} = 0.072 mmol/L. The reaction rate constant, k_d, was calculated to be 0.04, 0.70, and 19.34 nm^2/min when C_{MPA}

(37) Alberty, R. A.; Silbey, R. J. *Physical Chemistry*; Wiley: New York, 1992.

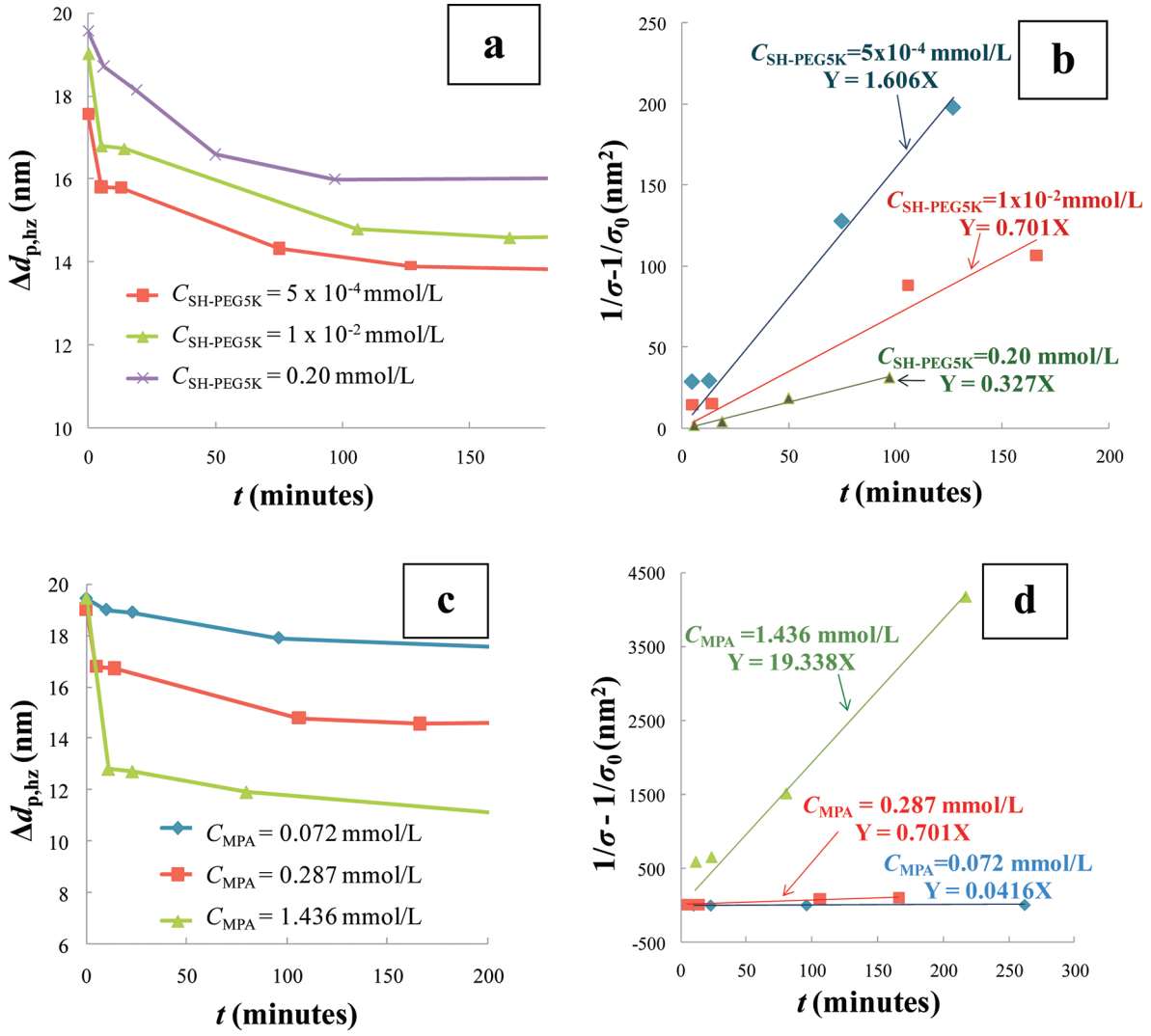

Figure 7. Kinetics of SH-PEG5K desorption from Au-NPs by displacement with MPA. (a) Change in particle size vs reaction time. Three different initial concentrations of SH-PEG5K were used: 5×10^{-4}, 1×10^{-2}, and 0.20 mmol/L. The concentration of MPA was 0.287 mmol/L. Lines are present to guide the eyes. (b) Second-order reaction kinetics for results in 7a. k_d can be calculated by using a linear correlation fit of $(1/\sigma - 1/\sigma_0)$ versus t. (c) Change in particle size vs reaction time. Three different initial concentrations of MPA were used: 0.072, 0.287, and 1.436 mmol/L. The concentration of SH-PEG5K was 1×10^{-2} mmol/L. Lines are present to guide the eyes. (d) Second-order reaction kinetics for results in 7c.

was 0.072, 0.287, and 1.436 mmol/L, respectively (Figure 7d). Increasing C_{MPA} results in increasing k_d values ($k_d \approx C_{SH-PEG5K}^{2.07}$).

4. Conclusions

DLS and ES-DMA have been successfully applied in parallel to characterize the competitive adsorption between SH-PEG5K and MPA on Au-NPs, a model three-component system. Because of the differences in molecular conformation and chain length, a significant increase in Au-NP size was observed after conjugating with SH-PEG5K, with almost no change in particle size after conjugating with MPA. The surface coverage of SH-PEG5K was assessed from the change in the dried (aerosol) particle mobility size measured by ES-DMA, and the results were used to derive an empirical correlation between surface coverage and increased hydrodynamic particle size obtained from DLS. A conceptual model was proposed to explain the surface conformation and surface coverage of SH-PEG under different environments, molecular concentrations, and relative molecular mass. DLS was found to be a very sensitive technique for characterizing surface coverage at low adsorption densities, with detection limits as low as 0.01 nm^{-2}. From the change in particle size measured by both DLS and DMA, the presence of MPA was shown to inhibit the adsorption of SH-PEG5K in the three-component system. Using the Langmuir equation, the equilibrium binding constants were quantified to show the extent of MPA inhibition on SH-PEG5K adsorption to Au-NPs. A kinetic study has also shown that MPA displaces SH-PEG5K from the surface of Au-NPs following a second-order reaction for SH-PEG5K desorption. These physical characterization techniques can also be used to study competitive adsorption between other molecules as long as the molecular conformations of the different components are distinct (e.g., long-chain PEG vs compact protein, such as TNF). Future work will seek to apply this approach to Au-NP-based three-component systems used in targeted cancer therapy. Through the quantitative study of particle−molecule interactions, as demonstrated in this study, parameters such as equilibrium binding constants and desorption rate constants can be obtained and then used to improve the formulation design and quality assurance of nanomedicine

products. The work presented here provides a proof of concept and demonstrates the efficacy of the complementary physical characterization approach for the investigation of molecular conjugation in nanoparticle systems.

Acknowledgment. We thank Dr. Anil Patri at the Nanotechnology Characterization Laboratory at the National Cancer Institute (NCL-NCI) for helpful discussions and research directions. This work was funded in part by NCI and the National Institutes of Health through an interagency agreement (Research to Support Characterization of Nanotechnologies for Cancer; NIH #Y1-CO-4118-002-000). We also thank Dr. Andrew Allen, Dr. Robert Cook, and Suvajyoti Guha at NIST for reviewing the article.